

1 **Supplementary Figures and Legends**

2 **Supplementary Figure S1. Intra-tumoral heterogeneity as shown by unsupervised clustering**

3 **and intra-sample subcluster level CNA profiles, related to Figure 1. (A)** UMAP visualization

4 of unsupervised clustering analysis of PCs at patient level in 48 patients with more than 50 PCs.

5 Patients were grouped by their diagnosis. **(B)** Heatmap showing genome wide inferred CNA

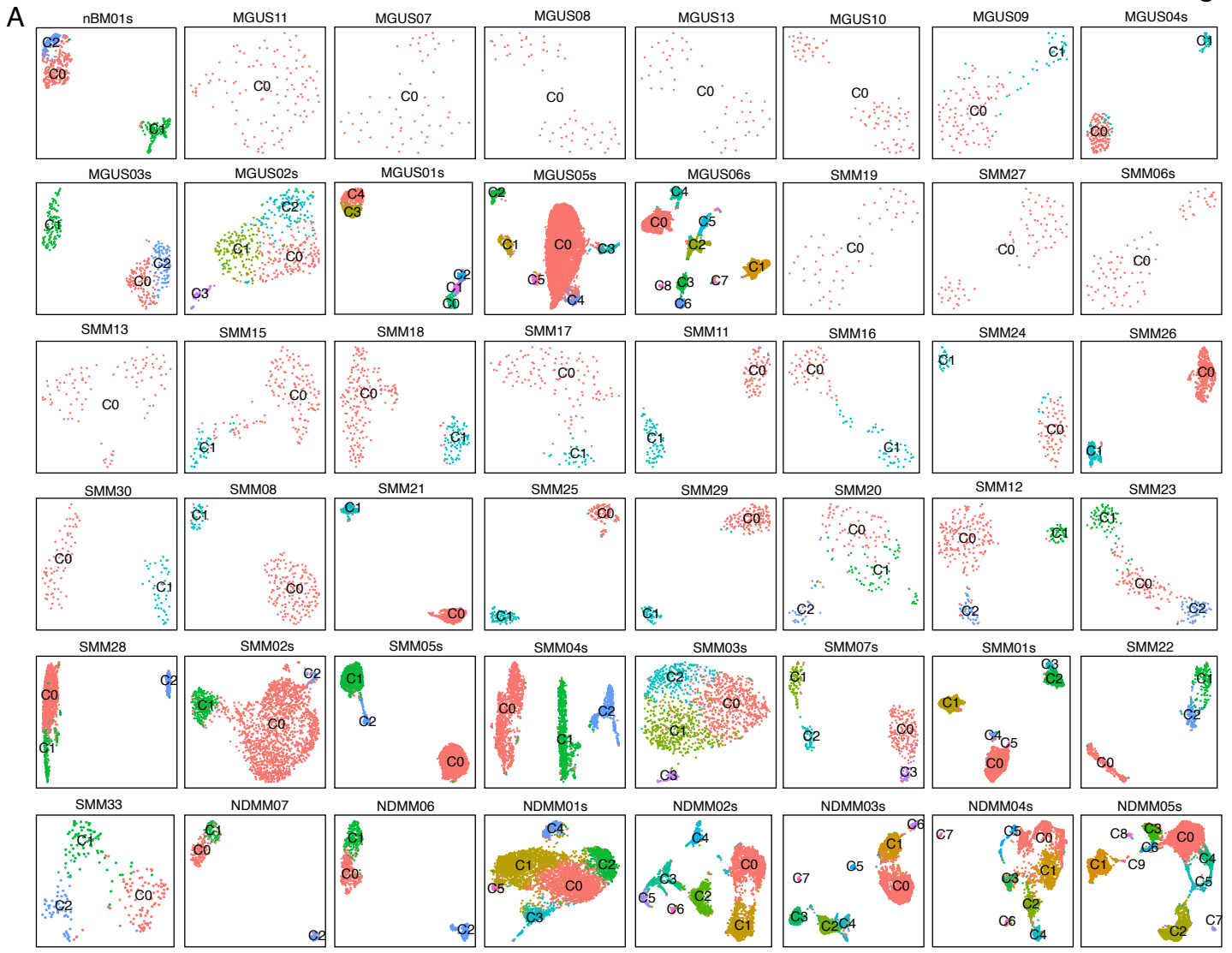
6 profiles for 150 PC clusters from 47 patients except the normal one. Clusters were firstly grouped

7 by their patient origins and then by diagnosis. Columns represent genomic regions, ordered by

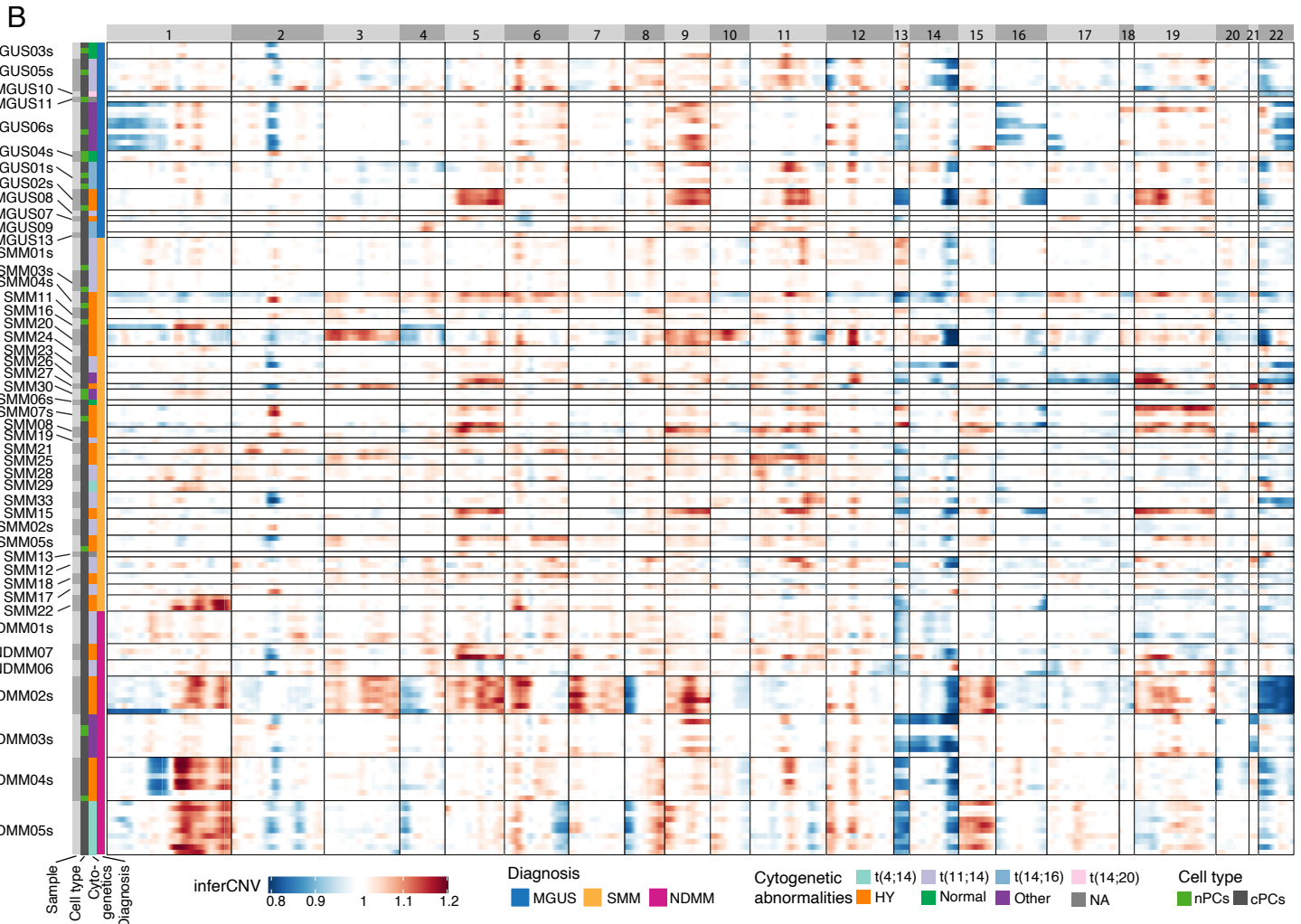
8 genome position across all chromosomes. Rows represent cluster averaged CNAs, with one row

9 per cluster.

10

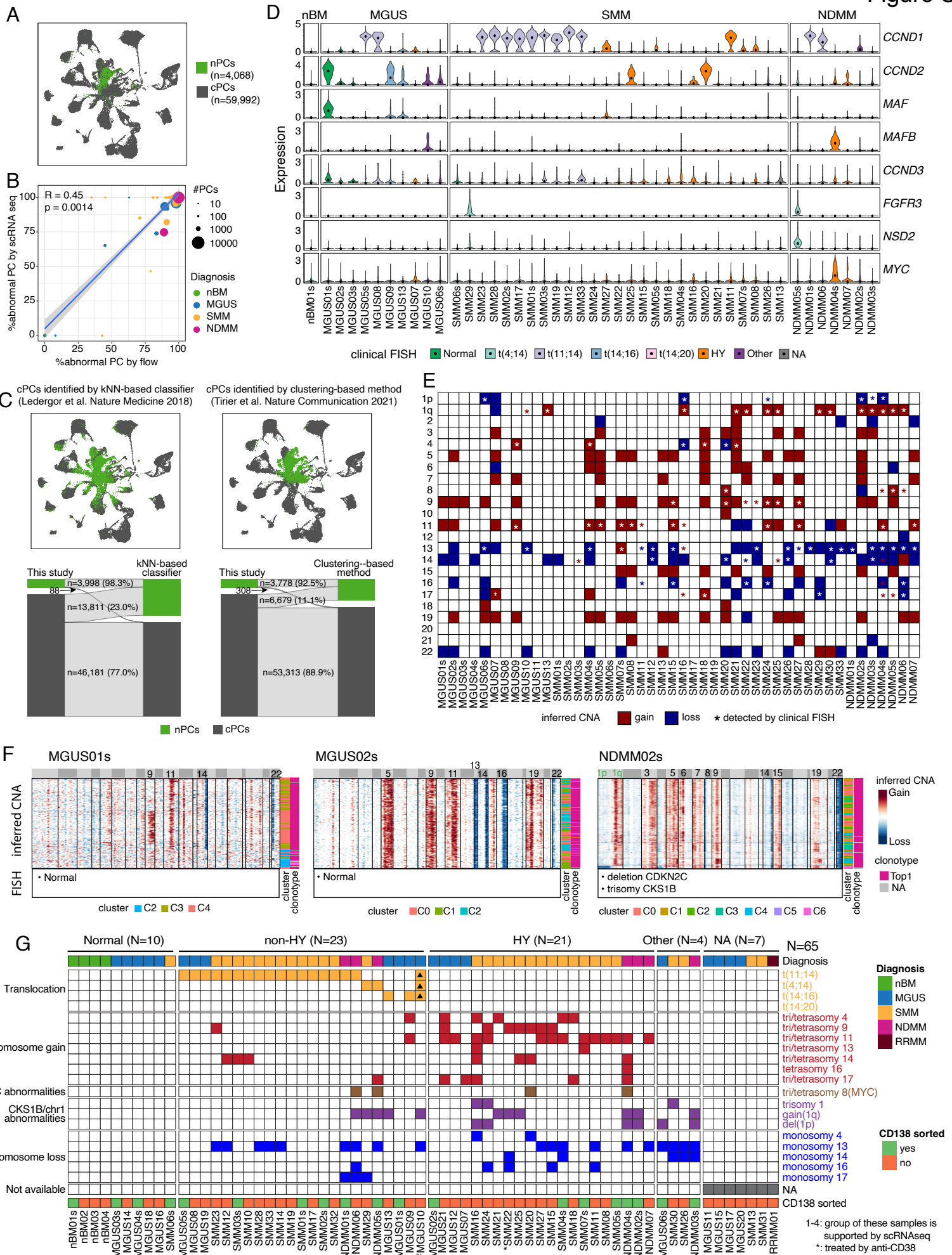


48 samples (1 nBM, 12 MGUS, 28 SMM, 7 NDMM), 153 intra-sample subclusters



11 **Supplementary Figure S2. Distribution of cells across patients, comparison of FISH and**  
12 **scRNAseq for abnormalities detection, and determination of genomic drivers of**  
13 **transformation for each patient, related to Figure 1. (A)** UMAP visualization of unsupervised  
14 clustering analysis of all PCs (n = 64,078) from 48 patients with more than 50 PCs. Cells were  
15 color coded by normal or clonal. **(B)** Comparison of proportion of abnormal plasma cells in all  
16 plasma cells measured by scRNAseq and flow cytometry. **(C)** UMAP showing the distribution of  
17 cPCs identified by KNN-based classifier (top left) or clustering-based method (top right). Alluvial  
18 plot at the bottom showed true positive, false negative, true negative, false negative of KNN-based  
19 (bottom left) or clustering-based (bottom right) method for identifying cPCs when using the results  
20 in this study as truth. **(D)** Violin plots showing expression of translocation related genes in cPCs  
21 in 44 patients or in nPCs in 1 healthy donor as shown in Fig. 1E but grouped by their diagnosis  
22 and color coded by their cytogenetic abnormalities determined by clinical FISH. **(E)** Comparisons  
23 of chromosome abnormalities detected by clinical FISH and scRNAseq. Chromosome and arm  
24 level gain and loss from scRNAseq were visually judged from inferred CNA profiles. **(F)**  
25 Comparisons of FISH results and inferred copy number alternation profiles from single cell RNA  
26 sequencing data for MGUS01s, MGUS02s and NDMM02s. Chromosome regions with obvious  
27 CNAs were labelled on the top. **(G)** Fluorescence in situ hybridization (FISH) results of 65 samples  
28 in this study as shown in Fig. 1B but grouped by their cytogenetic abnormalities.

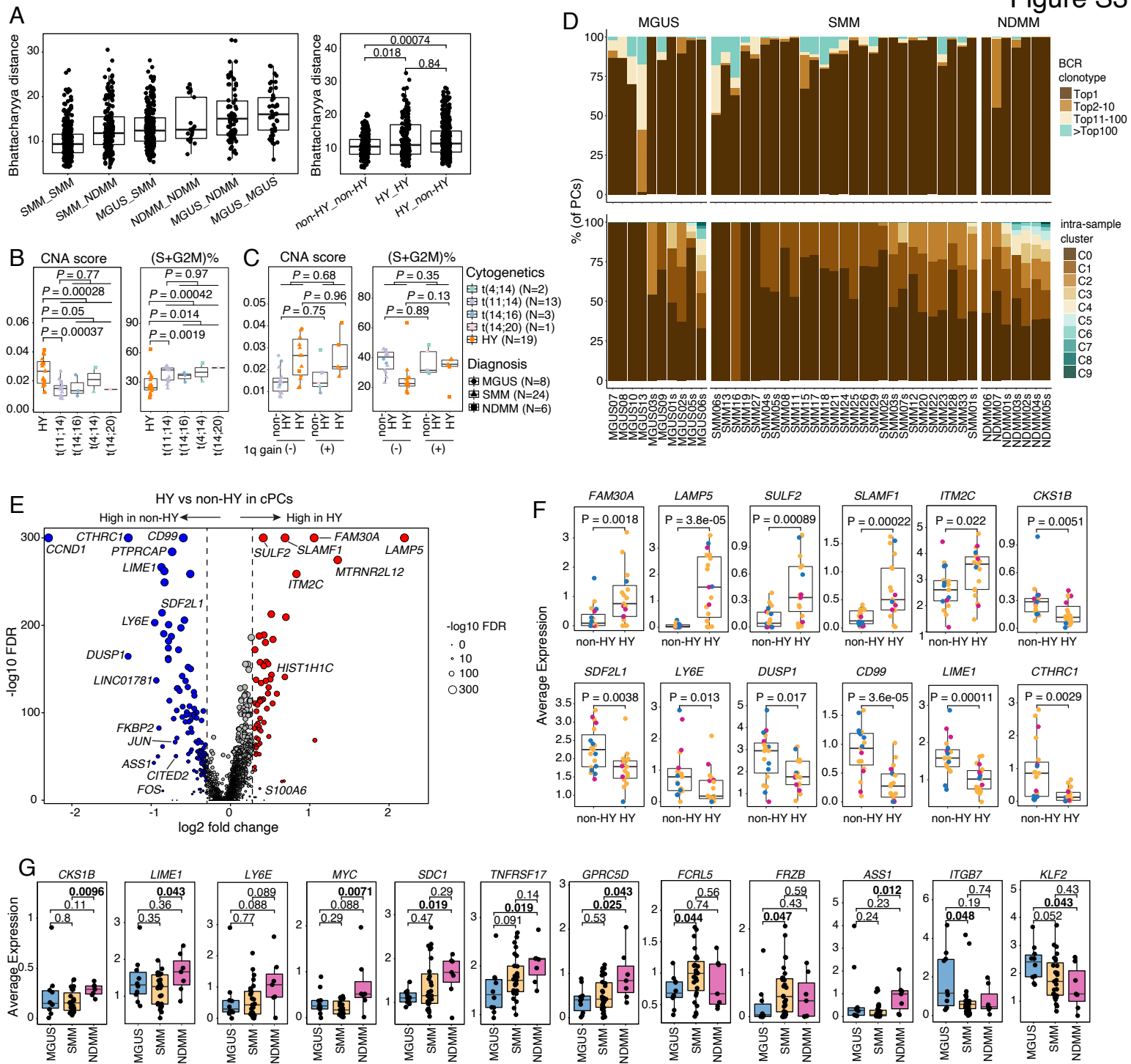
29





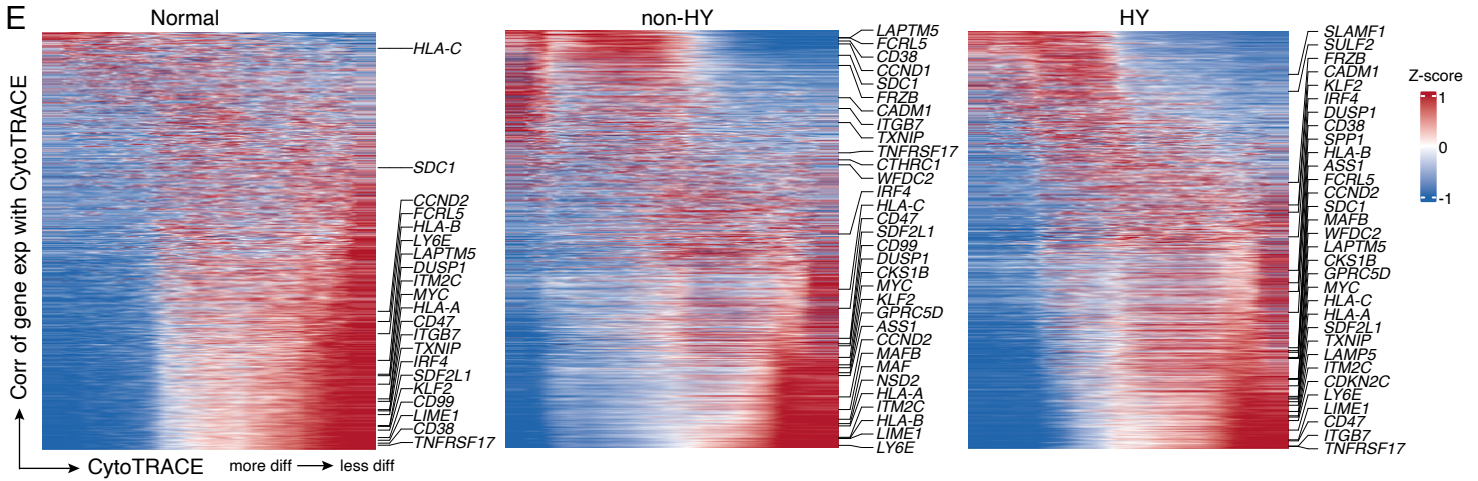
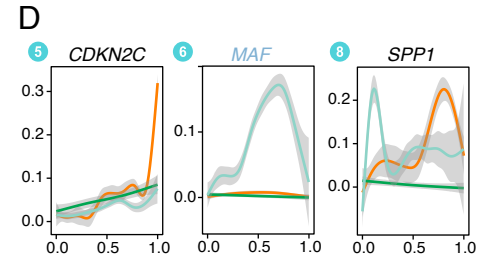
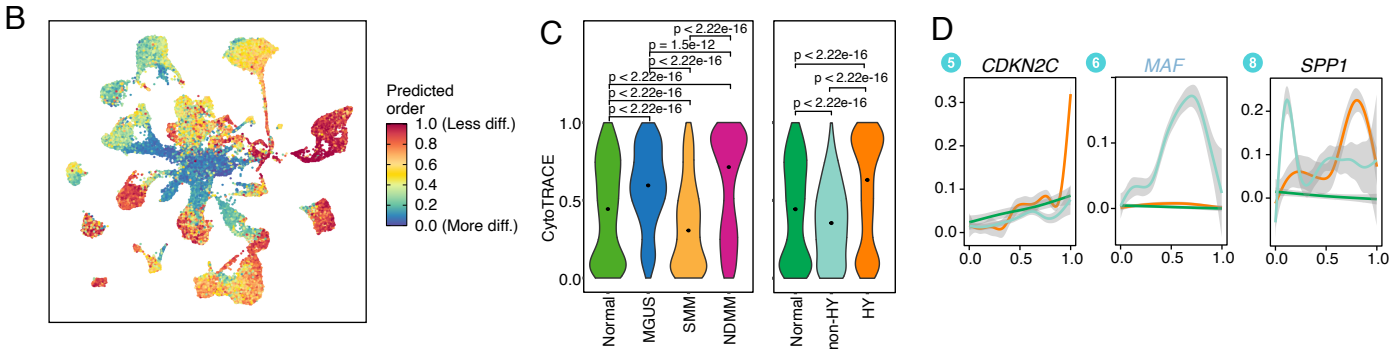
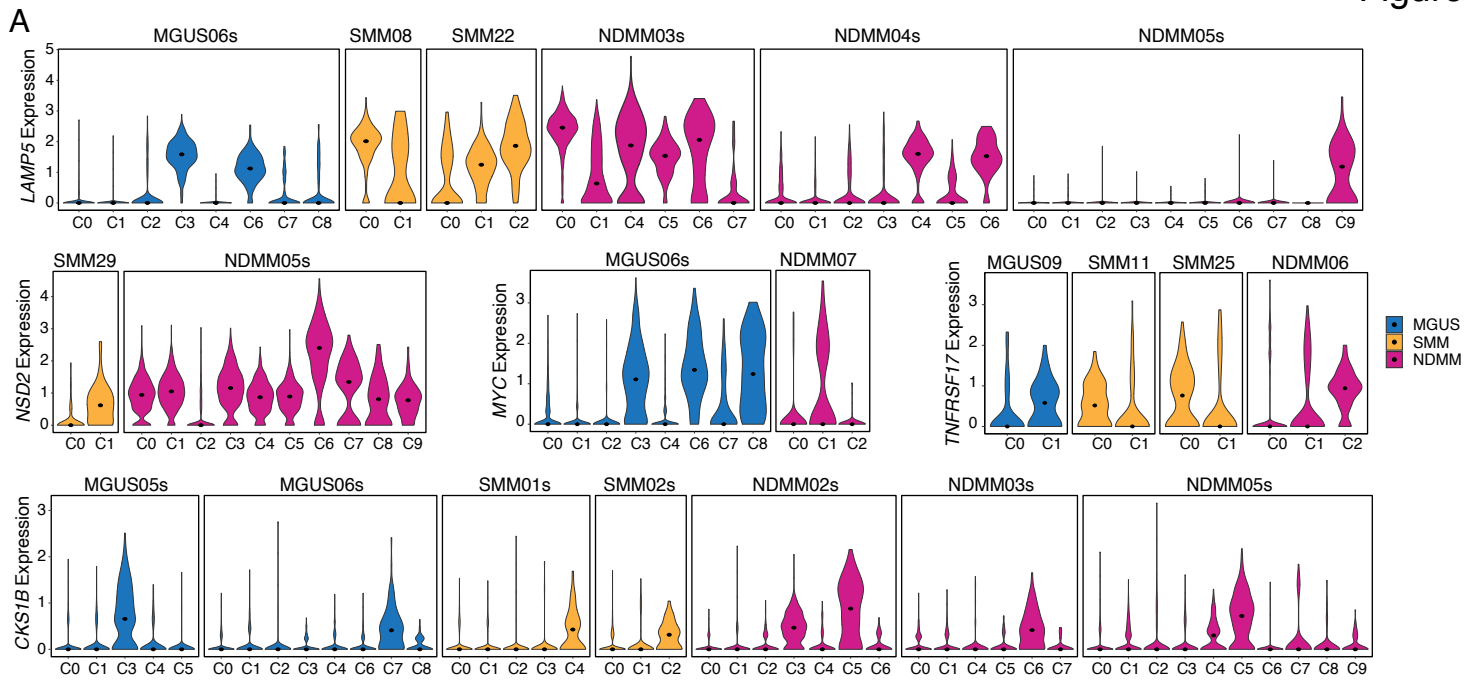
30 **Supplementary Figure S3. Characterization of cPCs, related to Figure 2.** (A) Boxplot showing  
31 the comparisons of Bhattacharyya distance between different diagnosis or cytogenetics groups.  
32 Groups were ordered by their median values. (B) Boxplots showing the comparisons of sample-  
33 averaged CNA score and proportion of cells at S and G2M phase between HY and different  
34 translocation groups. Dots were color coded by their cytogenetic abnormalities and shape coded  
35 by diagnosis. (C) Boxplots showing the comparisons of sample-averaged CNA score and  
36 proportion of cells at S and G2M phase between samples with (N=10) and without (N=28) 1q gain.  
37 Dots were color coded by their cytogenetics abnormalities and shape coded by disease stages. (D)  
38 Stacked bar charts showing BCR clonotype (upper) and intra-sample subcluster (lower)  
39 distributions in each sample grouped by disease stage. Clonotypes were grouped and colored by  
40 clonotype frequency categories. (E) Volcano plots of differentially expressed genes between cPCs  
41 from non-HY samples and HY samples. FDR, two-sided Wilcoxon rank sum test with Bonferonni  
42 correction. Dashed line,  $\log_2FC > 0.3$  or  $< -0.3$ . Labels, top ranked DEGs based on  $\log_2FC$ . (F)  
43 Boxplots showing the comparisons of averaged expression of top DEGs in cPCs between non-HY  
44 (N=19) and HY (N=19) at sample level. Dots were color coded by diagnosis. (G) Boxplots  
45 showing the comparisons of averaged expression of MM related key genes in cPCs between  
46 MGUS (N=10), SMM (N=27) and NDMM (N=7).

47



48 **Supplementary Figure S4. Dynamics of oncogene expression, related to Figure 3. (A)** Violin  
49 plots showing expression of *LAMP5*, *NSD2*, *MYC*, *TNFRSF17* and *CKS1B* in subclusters of related  
50 samples. **(B)** UMAP visualization of all PCs color coded by CytoTRACE score. **(C)** Violin plots  
51 showing distribution of CytoTRACE scores in cells with different disease stages and different  
52 cytogenetic abnormalities. **(D)** Two-dimensional plots showing the dynamic changes in expression  
53 levels of *CDKN2C*, *MAF* and *SPPI* (which show very low expression level) along the  
54 CytoTRACE score. Shaded band, 95th confidence interval. **(E)** Heatmap showing the expression  
55 of the top 2,000 highly variable genes along the CytoTRACE score in normal, non-HY and HY  
56 cells separately. Genes were ordered by their correlation with CytoTRACE score. Genes in (A)  
57 were labelled on the right.

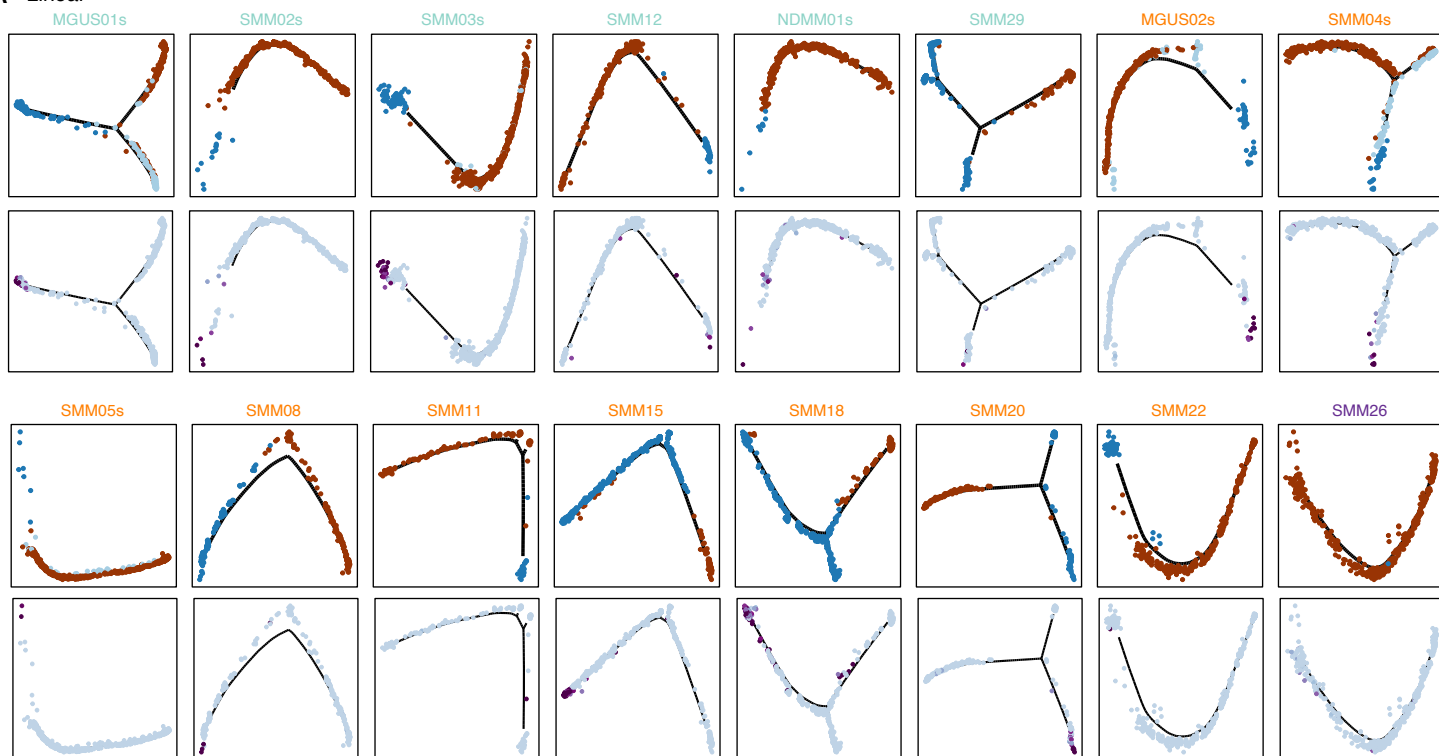
58



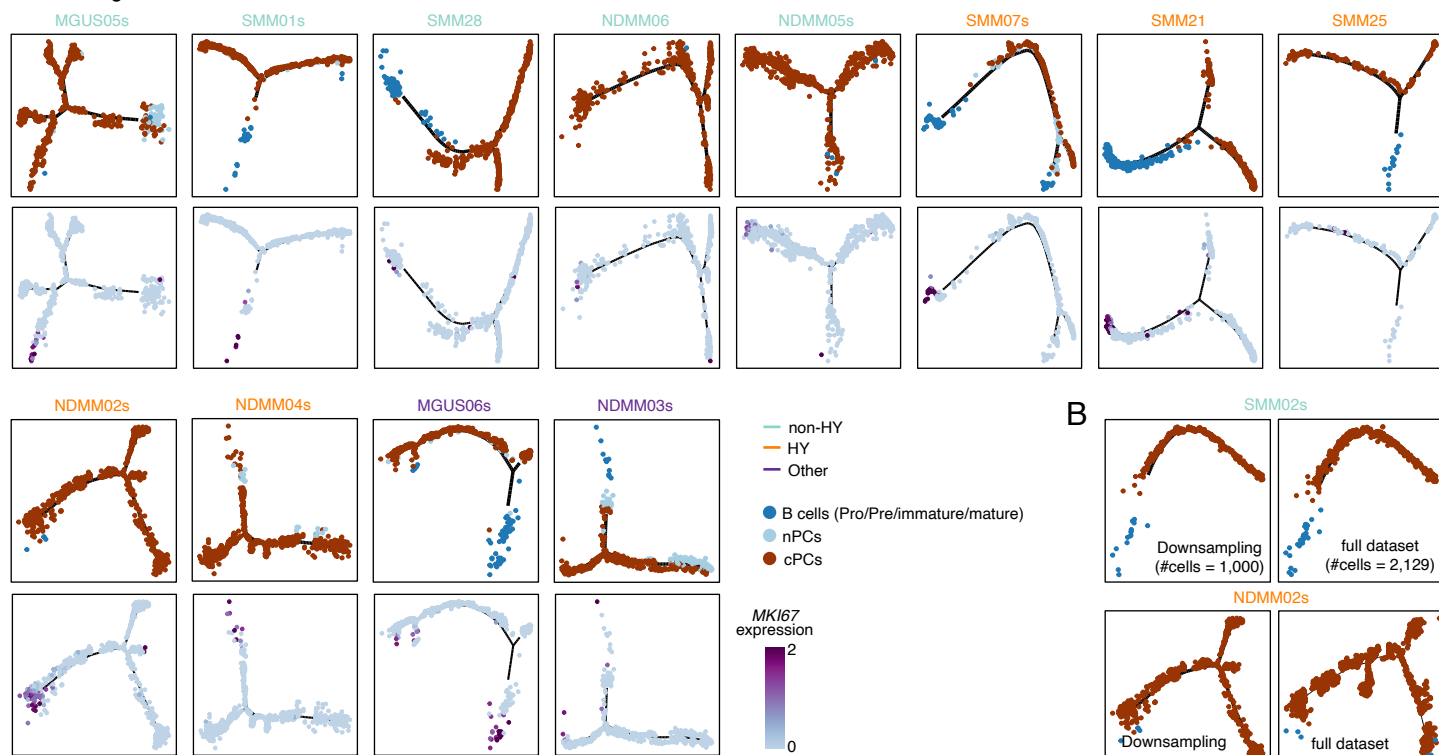
59 **Supplementary Figure S5. Pseudotime trajectory analysis of B lineage cells, related to**  
60 **Figures 4 and 5. (A)** Trajectories reconstructed using Monocle2 with cell type and expression of  
61 *MKI67* mapped on. Samples were grouped by visually inferred evolution patterns and sample  
62 names were color coded by their cytogenetic abnormalities. Only samples with more than 100  
63 cPCs and 2 subclusters were shown. **(B)** Down-sampling pseudotime trajectory analysis of  
64 SMM02s and NDMM02s.

65

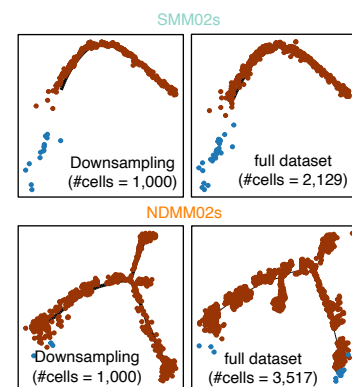
A



Branching



B

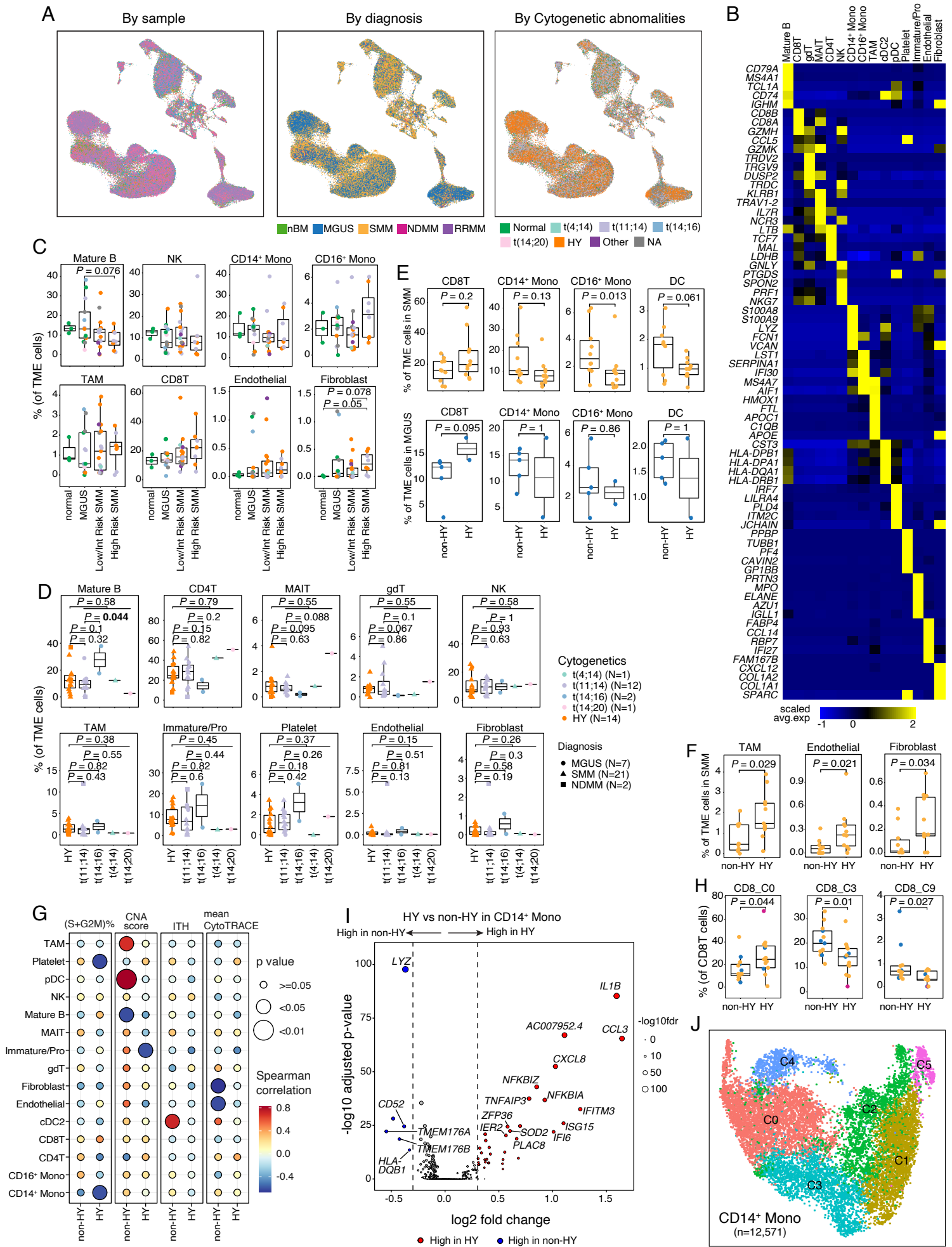


66 **Supplementary Figure S6. Landscape of tumor microenvironment, related to Figure 6. (A)**  
67 UMAP visualization of unsupervised clustering analysis of all TME cells (n = 120,677). Cells  
68 were color coded for their corresponding patient origins, diagnosis, and cytogenetic abnormalities.  
69 **(B)** Heatmap showing the scaled expression level of top 10 DEGs in the major cell types in TME.  
70 **(C)** Boxplots showing the comparisons of major cell type proportions among TME cells between  
71 nBM (N=3), MGUS (N=13), low/intermediate risk SMM (N=17) and high risk SMM (N=8). Dots  
72 are color coded by their cytogenetics abnormalities. Comparisons with  $P < 0.1$  are labeled. **(D)**  
73 Boxplots showing the comparisons of proportion of major cell types in TME between HY (N=14)  
74 and different translocation groups. Dots were color coded by their cytogenetic abnormalities and  
75 shape coded by diagnosis. **(E)** Boxplots showing the comparisons of proportion of CD8<sup>+</sup> T cells,  
76 CD14<sup>+</sup> monocytes, CD16<sup>+</sup> monocytes and DCs in TME between non-HY SMM (N=10) and HY  
77 SMM (N=11) samples (upper panel) and between non-HY MGUS (N=5) and HY MGUS (N=2)  
78 samples (lower panel). **(F)** Boxplots showing the comparisons of proportion of TAMs, Endothelial  
79 and Fibroblasts in TME between non-HY SMM (N=10) and HY SMM (N=11) samples. **(G)**  
80 Bubble plot showing the correlation of TME cellular compositions with ITH score, sample-  
81 averaged CNA score, proportion of cells at S and G2M phase, and sample-averaged CytoTRACE  
82 score of cPCs in non-HY and HY samples separately. **(H)** Boxplots showing the pairwise  
83 comparisons of proportion of CD8 T cell sub-clusters in CD8 T cells between non-HY (N=15) and  
84 HY (N=13) samples. Only sub-clusters reaching statistical significance were shown. **(I)** Volcano  
85 plots of differentially expressed genes in CD14<sup>+</sup> monocytes between non-HY and HY samples.  
86 FDR, two-sided Wilcoxon rank sum test with Bonferonni correction. Dashed line,  $\log_2FC > 0.3$   
87 or  $< -0.3$ . Labels, biologically important genes. **(J)** Uniform manifold approximation and



88 projection (UMAP) visualization of unsupervised sub-clustering analysis of CD14<sup>+</sup> Monocytes (n  
89 = 12,571).

90



91 **Supplementary Figure S7. Cell-cell interactions between cPCs and TME cells, related to**  
92 **Figure 7. (A)** Heatmap showing the number of interactions between each major cell types (#cells  
93 > 1000) inferred by CellphoneDB in non-HY and HY samples separately. **(B)** Bubble plot showing  
94 the expression (color key) and frequency (size key) of each ligand and receptor in corresponding  
95 cell types in non-HY and HY side by side. Only pairs in Fig 6I are shown. **(C)** Boxplots showing  
96 the comparisons of expression of *ICAMI* between NHPD (non-HY) and HPD (HY) in MMRF-  
97 COMMPASS cohort.

